Structural insights into how metallochaperones UreE and UreG interact to deliver a toxic metal to urease

Chun-Long Chan, Longson Tsz Hin Pang, Tung Choi, Ka-Chun Chan, Ka Lung Tsang, Ka Ming Lee, Kam-Bo Wong*

School of Life Sciences, Centre for Protein Science and Crystallography, State Key Laboratory of Agrobiotechnology, The Chinese University of Hong Kong, Hong Kong, China

*To whom correspondence should be addressed. Email: kbwong@cuhk.edu.hk

Address: Room 289, Science Centre, School of Life Science, The Chinese University of Hong Kong, Shatin, Hong Kong, China

Author contribution: K.B.W., K.L.T. designed research; C.L.C., L.T.H.P., T.C., K.C.C., K.L.T., K.M.L., K.B.W. performed research; C.L.C., T.C., K.C.C., K.B.W. analyzed data; C.L.C. and K.B.W. wrote the paper.

Abstract

Maturation of urease, a virulence factor for *Helicobacter pylori* infection, requires the delivery of nickel ions to the metalloenzyme. To avoid cytotoxicity, nickel ions are transferred within protein complexes of metallochaperones to ensure that the toxic metal do not escape into the cytoplasm. In the urease maturation pathway, metallochaperone UreG receives its nickel ions by forming a 2:2 complex with another metallochaperone UreE. Using C-terminal truncation variants of UreE [UreE(1-158) and UreE(1-148)], we determined the crystal structures of the $UreE_2G_2$ complex bound with nickel ions and GMPPNP, a non-hydrolysable GTP analogue. UreE-UreG interactions are asymmetric, where the UreG dimer mainly interacts with the proximal UreE. GTP binding induces conformational changes in the G2 and CPH motifs of distal UreG that enable its anchorage to the $UreE_2G_2$ complex. His68 of distal UreG moves towards and chelates a nickel ion at the UreE binding site. Formation of the $UreE_2G_2$ complex juxtaposes the nickel binding sites of UreE and UreG. Nickel transfer from UreE to UreG induces conformational changes that weaken UreE-UreG interactions, thereby facilitating UreG dissociation. We further demonstrated that the hydrogenase maturation factor HypA, providing the nickel source, could activate urease in vitro through protein-protein interaction with wild-type UreE but not with its truncation variants. UreG binding induces conformational changes in the C-terminal tail of UreE, promoting dissociation of HypA-UreE complex. Our work presents a paradigm on how GTP and nicking binding allosterically regulate the formation of a metallochaperone complex to facilitate nickel transfer.

45 **Significance**

46 Our work provides insights into how cells solve the problem of trafficking a toxic metal,
47 nickel, to the active site of urease. Colonization of *Helicobacter pylori* in acidic human
48 stomach requires the biosynthesis of active urease, which involves the delivery of the toxic
49 nickel ions to the active site of the metalloenzyme. To avoid cytotoxicity, nickel ions are
50 transported from one metallochaperone to another via the formation of protein complexes so
51 that the toxic metal ions do not escape into the cytoplasm. Supported by structural and
52 biochemical evidence, we present a paradigm on how GTP and nickel binding allosterically
53 promote the formation of a complex between metallochaperones UreE and UreG to facilitate
54 nickel transfer between the two proteins.

55

56 **Introduction**

57 *Helicobacter pylori* infects half of the human population and is associated with an
58 increased risk of peptic ulcers and gastric cancer (1). *H. pylori* is the only pathogen that can
59 colonize the acidic human stomach because it produces large amount of urease, which
60 hydrolyze urea into ammonia that helps the bacterium to maintain an intracellular neutral pH
61 (2). The urease is a nickel (Ni) enzyme containing two Ni(II) ions in the active site (3, 4). The
62 apo-urease is inactive, and biosynthesis of active urease requires a maturation process that
63 deliver the nickel ions to the active site of urease (5).

64 Nickel ion is cytotoxic as it can displace weaker ions such as magnesium ions in the
65 active site of essential enzymes like GTPases (6). As a result, the metal ion is tightly regulated
66 so that there are essentially no free nickel ions in the bacterial cells (7, 8). The urease
67 maturation pathway represents a paradigm on how cells solve the problem of delivering a
68 toxic metal ion from one protein to another. To avoid cytotoxicity, cells have evolved
69 metallochaperones, or metal carrier proteins, to transport Ni(II) ions (5). There are four urease
70 accessory proteins that are involved in the nickel delivery to the urease: UreD (formerly
71 called UreH), UreE, UreF and UreG (Fig. 1A). UreE is a homodimer that can bind a Ni(II)
72 ion at the dimeric interface with a conserved GNRH motif (9-11). UreG is a SIMIBI (Signal
73 recognition particle, MinD and BioD) GTPase that can undergo Ni/GTP-dependent
74 dimerization that chelates a Ni(II) ion in a square-planar geometry with a conserved CPH
75 motif at the dimeric interface (12, 13). UreF and UreD forms a UreFD complex that interacts
76 GDP-bound UreG to form a 2:2:2 heterotrimeric UreGFD complex (12, 14). In the presence
77 of GTP, UreG dissociates from the UreGFD complex and forms a $UreE_2G_2$ complex with
78 UreE (13, 15) (Fig. 1A). After receiving its nickel ions from the $UreE_2G_2$ complex, UreG then
79 forms an activation complex with UreFD and apo-urease. Upon GTP hydrolysis, the nickel

80 ion is released from UreG, pass through a protein tunnel within the activation complex, and
81 reach the active site of urease (16) (Fig. 1A).

82 To avoid the toxic nickel ion escaping into the cytoplasm, nickel ions are delivered
83 within protein complexes. The specificity of nickel transfer is determined by protein-protein
84 interactions – nickel ions are delivered from UreE to UreG and then to urease via the
85 formation of the $UreE_2G_2$ complex and the activation complex (Fig. 1A). Our previous
86 structural studies of protein complexes along the urease maturation pathway – UreFD (14),
87 UreGFD (12), Ni-bound UreG dimer (13) and UreFD/apo-urease complexes (16) – have
88 provided insights into how nickel ions are transferred from UreG to urease via the formation
89 of the activation complex. To shuttle the nickel ions from one protein complex to another,
90 UreG must switch protein binding partners from the UreGFD complex to form the $UreE_2G_2$
91 complex and then dissociates from the complex after nickel transfer.

92 The molecular mechanism on how UreE and UreG interact to facilitate urease maturation
93 is not fully understood. Here, we fill the knowledge gap by solving the crystal structures of
94 the $UreE_2G_2$ complex bound with Ni(II) and guanosine 5'-(β,γ-imido) triphosphate
95 (GMPPNP), a non-hydrolysable analogue of GTP. The structures reveal GTP-dependent
96 conformational changes that explain why UreG, in its GTP bound state, prefers to form a 2:2
97 complex with UreE, and how nickel transfer from UreE to UreG may weaken the UreE-UreG
98 interaction, thereby promoting UreG dissociation from the $UreE_2G_2$ complex. Complemented
99 by mutagenesis and biochemical analyses, we further showed that UreG binding induces
100 conformational changes in the C-terminal tail of UreE, which is important for interacting with
101 the hydrogenase maturation factor HypA but not for interacting with UreG.

102

103

104 **Results**

105 **Crystal structure of $UreE_2G_2$ in complex with Ni(II) and GMPPNP**

106 *H. pylori* UreE contains a C-terminal tail that is not conserved in other species (Fig. 1G).
107 It has been previously shown that truncation of residues 158-170 did not affect the formation
108 of the $UreE_2G_2$ complex (15). To determine the crystal structures of the $UreE_2G_2$ complex, we
109 created two truncation variants of UreE: UreE(1-158) and UreE(1-148) containing residues 1-
110 148 and 1-158 residues, respectively. $UreE_2G_2$ complexes were obtained by mixing the UreE
111 variants with *H. pylori* UreG in 1:1 molar ratio in the presence of Ni(II) ions and GMPPNP, a
112 non-hydrolysable GTP analogue.

113 The UreE(1-158) complex crystallized in space group $P2_1$ with unit cell dimensions of
114 70.17 × 166.60 × 154.02 Å, α=γ=90°, β= 90.44° (Table S1). Diffraction data were collected to
115 3.1 Å resolution and the structure was solved by molecular replacement using the crystal
116 structure of UreE (11) as the search template combined with single-wavelength anomalous
117 diffraction (MR-SAD). The UreE(1-158) forms a 2:2 complex with UreG, and four copies of
118 $UreE(1\text{-}158)_2G_2$ complexes were found in the asymmetric unit (Fig. 1B). The $UreE(1\text{-}148)_2G_2$
119 complex crystallized in space group $P2_1$ with unit cell dimensions of 70.97 × 151.07 × 83.15
120 Å, α=γ=90°, β= 99.50° (Table S1). The structure of $UreE(1\text{-}148)_2G_2$ complex was determined
121 to 2.8 Å resolution by molecular replacement using the structure of $UreE(1\text{-}158)_2UreG_2$ as the
122 search template. Two copies of $UreE(1\text{-}148)_2G_2$ complexes were found in the asymmetric unit
123 (Fig. 1C).

124 UreE folds into an N-terminal (NTD) and a C-terminal (CTD) domains (Fig. 1D and 1G).
125 The CTD is responsible for dimerization of UreE (Fig. 1E). UreG adopts a SIMIBI-GTPase
126 fold with a seven-stranded β-sheet and ten α-helices (Fig. 1D). The conserved G1-G5 motifs
127 involved in nucleotide binding and GTP-dependent conformational changes are identified in

128 Fig. 1D and 1H.

129 **UreE forms an asymmetric complex with UreG**

130 In the crystal structure, UreE forms an asymmetric 2:2 complex with UreG (Fig. 1E).
131 UreG forms a dimer that docks to the proximal UreE in a such way that the long axes of UreE
132 and UreG dimers are oriented at an angle of ~45° (Fig. 2A). The structures of UreE and UreG
133 protomers in the UreE(1-148)$_2$G$_2$ complex are superimposable to those in the UreE(1-158)$_2$G$_2$
134 complex (Fig. S1). In addition, the structures of both UreE protomers are similar, except that
135 the C-terminal residues 148-155 are structured in the proximal UreE but are disordered in the
136 distal UreE (Fig. S1A). Structures of distal UreG only differ from those of proximal UreG in
137 the CPH metal-binding motif (Cys66-Pro67-His68) (Fig. S1B), in which His68 of distal UreG
138 move towards UreE and, together with His102 of UreE, chelates a nickel ion at the
139 UreE/UreG interface (Fig. 1F and S2A). One GMPPNP is bound to each of the proximal and
140 distal UreG and the magnesium ion binding sites of UreG are occupied by the excess nickel
141 ions used in the crystallization (Fig. S2B).

142 The interactions between UreE and UreG are asymmetric, with residues of proximal
143 UreE making most of the interactions with UreG (Fig. 2B). Proximal UreE forms a number of
144 hydrogen bonds and salt bridges with proximal and distal UreG (Fig. S3). His102 is the only
145 residue from distal UreE involved in UreE-UreG interactions. This residue, together with
146 His102 of proximal UreE and His68 of distal UreG, chelates a nickel ion at the UreE-UreG
147 interface (Fig. 1F). In addition to polar interactions, Leu197 of proximal UreG docks to a
148 hydrophobic pocket form by Ile2, Ile34, Arg36, Ala46, Arg48 (Fig. S4).

149 **GTP-dependent conformational changes promote binding of distal UreG to the UreE$_2$G$_2$**
150 **complex**

151 We have previously shown that UreG prefers to form a UreGFD complex in its GDP-

152 bound state, but switches to form a $UreE_2G_2$ complex in the presence of GTP (13). To
153 understand the GTP-dependent conformational changes that promote the formation of the
154 $UreE_2G_2$ complex, we compare structures of proximal and distal UreG to that of the GDP-
155 bound UreG in the UreGFD complex (12) (Fig. 3A). Binding of GMPPNP induces
156 conformational changes in the G2 motif and helix-2 of both proximal and distal UreG.
157 Additional conformational changes are found in the CPH motif in distal UreG (Fig. 3A).
158 GTP-dependent conformational changes are initiated by charge repulsion between the γ-
159 phosphate of GMPPNP and Asp37 of the G2 motif (Fig. 3B). As a result, Asp37 is pushed
160 away from the nucleotide binding site, causing structural rearrangement in the G2 motif and
161 helix-2. In distal UreG, Tyr39 and Gly65 moves towards and form hydrogen bonds with
162 Glu119 of proximal UreE (Fig. 3B). Nickel binding promotes additional conformational
163 changes in the CPH motif of distal UreG – His68 and Asp74 move towards UreE where they
164 interact with the bound nickel ion and Arg101 of proximal UreE, respectively (Fig. 3B). In
165 addition, conformational changes in the G2 motif causes helix-2 to tilt towards the nucleotide
166 binding site, bringing Glu42 and Asp43 of UreG to form inter-subunit salt-bridges with
167 Arg130 and Lys131 of the opposite UreG protomer (Fig. 3C).

168 We noticed that the G2 motif of proximal UreG is far away from the UreE-UreG
169 interface (Fig. S5). Since the GTP-dependent conformational changes are localized in the G2
170 motif of proximal UreG (Fig. 3A), we argue that the proximal UreG in its GDP-bound state
171 should be able to bind UreE, justifying the observation that UreE forms a 2:1 $UreE_2G$
172 complex with UreG in the presence of GDP (15). On the other hand, GTP-dependent
173 conformational changes cause distal UreG to form extra interactions with UreE (Fig. 3B) and
174 with proximal UreG (Fig. 3C), explaining why GTP binding promotes the anchorage of distal
175 UreG to form the $UreE_2G_2$ complex.

176 **Formation of $UreE_2G_2$ complex induces conformational changes in the NTD and C-**
177 **terminal tail of proximal UreE**

178 The structures of proximal and distal UreE in the $UreE_2G_2$ complex were compared to
179 the crystal structure of the Ni-bound UreE dimer (11). Structural superimposition reveals
180 conformational changes in the NTD and C-terminal tail of proximal UreE (Fig. 4A). As
181 shown earlier, Leu197 of proximal UreG forms hydrophobic contacts with a pocket composed
182 of Ile2, Ile34, Arg36, Ala46 and Arg48 on proximal UreE (Fig. S4). Upon formation of the
183 $UreE_2G_2$ complex, the NTD of proximal UreE undergoes a domain movement that positions
184 these residues to interact with Leu197 of proximal UreG (Fig. 4B).

185 On the other hand, in the structure of Ni-bound UreE dimer, His152, together with
186 His102 from both protomers, binds a nickel ion at the dimeric interface (11). Binding of UreG
187 in the $UreE_2G_2$ complex causes the C-terminal tail (149-155) of proximal UreE to swing
188 outward such that His152 forms a hydrogen bond with Asp74 of proximal UreG (Fig. 4C).

189 To further assess the role of the C-terminal residues of UreE in nickel delivery, we have
190 prepared Ni-bound UreE or its truncation variants and test if they can activate urease in the
191 presence of UreGFD and a reaction buffer containing GTP and $KHCO_3$ (Fig. 4D). We also
192 included apo-forms of UreE as negative controls. Our results show that Ni-bound wild-type
193 UreE, UreE(1-158) and UreE(1-148), but not their apo-forms, can activate urease in vitro.
194 There was no significant difference between urease activated by wild-type UreE and UreE(1-
195 158), which is consistent with the observations that residues 156-158 of UreE, which are
196 disordered in the crystal structure of the $UreE(1\text{-}158)_2G_2$ complex, are not involved in binding
197 UreG (Fig. S6). On the other hand, urease activated by UreE(1-148) exhibited a lower activity,
198 suggesting that further removal of residue 149-158 would remove the interaction between
199 His152 of proximal UreE and Asp74 of proximal UreG, and thereby weaken UreE-UreG
200 interactions.

201 **Interaction between HypA and the C-terminal tail of UreE facilitates nickel transfer**
202 **between the hydrogenase and urease maturation pathway.**

203 How UreE receives its nickel ions from upstream sources is not fully understood. In
204 *Helicobacter* species, which contain both the [NiFe]-hydrogenase and urease, there are
205 accumulating evidence suggesting that UreE can receive its nickel ions by cross-talking with
206 the hydrogenase maturation pathway (5). Nickel delivery to the [NiFe]-hydrogenase is
207 facilitated by the hydrogenase maturation factors HypA and HypB. UreE can form a 2:1
208 complex with HypA (15, 17, 18).

209 To investigate whether UreE can receive nickel ions by protein-protein interaction with
210 HypA, we performed an in vitro urease activation assay using a two-chamber dialyzer. To
211 simplify protein purification, we attached a Strep-tag II sequence (WSHPQFEK) to the C-
212 terminus of HypA ($HypA_{str}$). We show that urease was activated only when Ni-bound $HypA_{str}$
213 was mixed with UreE, UreGFD and apo-urease in the same chamber of the dialyzers (Fig. 5A,
214 reaction 1), but not when Ni-bound $HypA_{str}$ was separated from the rest of the protein
215 components by a dialysis membrane (Fig. 5A, reaction 2). These observations suggest that Ni-
216 bound $HypA_{str}$ can provide the nickel source for urease activation via protein-protein
217 interaction, which is prevented by the dialysis membrane in the reaction 2 of Fig. 5A. Urease
218 activation was greatly reduced when UreE was placed in the left chamber and was separated
219 from the rest of the protein components (Fig. 5A, reaction 3), suggesting that HypA cannot
220 pass its nickel ions to protein components other than UreE. Taken together, our results
221 suggest that UreE receives its nickel ions from the hydrogenase maturation pathway by
222 interacting with HypA.

223 To further examine the interaction between HypA and UreE, we performed pull-down
224 assay by mixing UreE or its truncation variants with Ni-bound $HypA_{str}$ and loaded the mixture

225 to Strep-Tactin resins (Fig. 5B). We showed that wild-type UreE was co-eluted with $HypA_{str}$,
226 suggesting UreE can interact with HypA. In contrast, the interaction between the truncation
227 variants of UreE and $HypA_{str}$ was greatly reduced (Fig. 5B). These results demonstrate that
228 the C-terminal residues 159-170 of UreE is essential for its interaction with HypA.

229 To access whether the C-terminal residues of UreE is essential for nickel transfer from
230 HypA, we performed an in vitro urease activation assay, where Ni-bound $HypA_{str}$, providing
231 the sole nickel source for urease activation, was added to UreE or its truncation variants,
232 UreGFD and apo-urease. Apo-$HypA_{str}$ was also added as negative controls. Urease activation
233 was observed only when wild-type UreE with an intact C-terminal tail was present (Fig. 5C).
234 Taken together, our results suggest that truncation variants of UreE, lacking the essential C-
235 terminal residues required for interacting with HypA, failed to receive nickel ions from HypA
236 for urease activation (Fig. 5C).

237

238

239 **Discussion**

240 To deliver the toxic Ni(II) ion to the urease, cells have evolved metallochaperones to
241 transport the metal ions from one protein to another. To fulfill their roles in nickel trafficking,
242 metallochaperones must form specific protein complexes like the $UreE_2G_2$ complex to
243 facilitate metal transfer within the complex. They also need to develop a mechanism to
244 dissociate from the complex and switch protein binding partners so that they can shuttle the
245 metal ions to the next protein target along the urease maturation pathway.

246 The crystal structures of the $UreE_2G_2$ complex reported here show that GTP-dependent
247 conformational changes promote the formation of the $UreE_2G_2$ complex. UreE and UreG
248 form an asymmetric 2:2 complex, in which the proximal UreE makes most of the interactions
249 with the UreG dimer (Fig. 2). GTP binding induces conformational changes in the G2 motif
250 of both proximal and distal UreG that promote the dimerization of UreG (Fig. 3A & 3C). The
251 structural rearrangement in the G2 motif also causes Tyr39 to flip outward and make steric
252 clashes with UreF in the UreGFD complex (Fig. S7) (13), justifying the observation that GTP
253 binding promotes dissociation of UreG from the UreGFD complex (12, 13).

254 In distal UreG, the conformational changes bring Tyr39 to form a hydrogen bond with
255 Glu119 of proximal UreE (Fig. 3B). In addition, His68 of distal UreG moves towards the
256 nickel binding site of UreE, chelates a nickel ion with His102 of UreE and induces additional
257 conformational changes in the region near the CPH motif of distal UreG (Fig. 3B). As a result,
258 Gly65 and Asp74 of distal UreG form hydrogen bonds with Glu119 and Arg101 of proximal
259 UreE (Fig. 3B). Taken together, GTP binding induces conformational changes in both G2 and
260 CPH motifs, promoting additional interactions between distal UreG and the UreE dimer and
261 the formation of the $UreE_2G_2$ complex (Fig. 3). The role of GTP-dependent conformational
262 changes is also supported by a previous observation that the D37A/E42A variant of UreG,
263 which is defective in GTP-dependent dimerization, failed to switch from the UreGFD

264 complex to form the $UreE_2G_2$ complex (13).

265 Formation of the $UreE_2G_2$ complex facilitates nickel transfer by juxtaposition of the
266 nickel binding sites of UreE and UreG (Fig. 6A). We have shown previously that protein-
267 protein interaction between UreE and UreG is required for nickel delivery from UreE to
268 urease (13). Yang and co-workers showed that nickel ions are transferred from UreE to UreG,
269 but not in the reverse direction (15). UreG forms a dimer when bound to a nickel ion and GTP
270 (12, 13). The nickel ion is coordinated in a square planar geometry by Cys66 and His68 of the
271 CPH motif from each of the UreG protomers (13). In the structure of the $UreE_2G_2$ complex,
272 the nickel ion, coordinated by His102 of UreE and His68 of distal UreG, is located at the
273 nickel binding of UreE (Fig. S8). So, the structures reported here represent the structure of the
274 $UreE_2G_2$ complex before the transfer of nickel from UreE to UreG.

275 To understand the conformational changes in UreG upon transfer of nickel to UreG, we
276 compared the structure of the $UreE_2G_2$ complex to that of the Ni/GMPPNP-bound UreG
277 dimer. Notable differences are found in the CPH motif of distal UreG (Fig. S9) – Cys66 and
278 His68 of distal UreG move back to the nickel binding site of UreG to coordinate the nickel
279 ion at the dimeric interface of UreG (Fig. 6A). Tyr39, Gly65 and Asp74 of distal UreG move
280 away from the UreE-UreG interface, breaking hydrogen bonds with Glu119 and Arg101 of
281 proximal UreE (Fig. 6A). We argue that these conformational changes induced by nickel
282 transfer should weaken the UreE-UreG interaction and facilitate dissociation of UreG.

283 In *Helicobacter* species, UreE can get its upstream nickel ions by cross-talking with the
284 hydrogenase maturation pathway (5). Pioneer work by Maier's group shows that knocking out
285 *hypA* and *hypB* genes greatly reduced the activation of both [NiFe]-hydrogenase and urease in
286 *H. pylori* and *H. hepaticus* (19, 20). HypA and UreE can form a HypA-$UreE_2$ complex that
287 facilitates nickel transfer between the hydrogenase and urease maturation pathways (15, 17,

288 18). *H. pylori* expressing metal-binding defective mutants of HypA exhibit reduced urease
289 activation and are sensitive to acidic shock (21, 22). All these observations suggest the role of
290 HypA in urease activation in *H. pylori*.

291 Here, we provided direct evidence that nickel ions from HypA can be delivered to the
292 urease. We showed that urease was activated upon addition of Ni-bound HypA, providing the
293 sole source of nickel ions, to the protein components (UreE, UreGFD and apo-urease) of the
294 urease maturation pathway (Fig. 5A, reaction 1). Separating Ni-bound HypA and UreE by a
295 dialysis membrane in a two-chamber dialyzer greatly reduced urease activation in vitro (Fig.
296 5A, reactions 2 and 3), suggesting that HypA passes its nickel ion to UreE via protein-protein
297 interactions. We further showed that while removal of the C-terminal residues (159-170) in
298 UreE(1-158) did not affect nickel transfer from UreE to UreG (Fig. 4D), the truncations
299 abolished HypA-UreE interactions (Fig. 5B) and nickel transfer from HypA to UreE (Fig. 5C).

300 It has been shown that HypA could compete with UreG for binding UreE (23). UreE
301 prefers to form a complex with HypA in the absence of GTP but prefers to form a complex
302 with UreG upon addition of GTP (15). Then what causes UreE to switch protein binding
303 partners? Our work provides structural insights into how GTP-dependent conformational
304 changes promote UreG binding and dissociation of HypA from the HypA/$UreE_2$ complex. As
305 discussed, GTP binding induces conformational changes in the G2 and CPH motifs of distal
306 UreG, thereby promotes the anchorage of distal UreG to the $UreE_2G_2$ complex (Fig. 3). We
307 also show that UreG binding induces conformational changes in the residues 149-155 of the
308 proximal UreE, which move away from the nickel binding of UreE (Fig. 4C). Such a
309 movement likely promotes HypA dissociation as the C-terminal residues (159-170) are
310 essential in HypA-UreE interaction (Fig. 5B) (17, 24). In a model by Zambelli and co-
311 workers, the N-terminal MHE motif of HypA was predicted to coordinate a nickel ion at the
312 nickel binding site of UreE (24). As the distal UreG in the $UreE_2G_2$ complex also coordinate a

313 nickel ion at the same location (Fig. S8), the UreG binding is expected to make steric clashes
314 with HypA that promote its dissociation.

315 A summary on how conformational changes in the $UreE_2G_2$ complex facilitate urease
316 maturation is presented in Figure 6B and Supplemental Movie S1. GTP-dependent
317 conformational changes promote dimerization of UreG and binding of the UreG dimer to
318 UreE. UreG binding induces conformational changes in the C-terminal tail of UreE, which is
319 not essential for UreG binding but essential for HypA interaction, thereby promoting
320 dissociation of HypA. The UreE-UreG interactions are asymmetric, with proximal UreE
321 forming most of the interactions with both proximal and distal UreG. GTP-dependent
322 conformational changes in UreG are also asymmetric – additional conformational changes are
323 observed in the CPH motif of distal UreG, where His68 moves toward and chelates a nickel
324 ion at the binding site of UreE. Nickel transfer from the binding site of UreE to UreG induces
325 conformational changes in distal UreG that weaken the UreE-UreG interactions, and facilitate
326 dissociation of Ni-bound UreG dimer. After dissociation from the $UreE_2G_2$ complex, the
327 UreG dimer then delivers its nickel ion to the urease via the formation of an activation
328 complex with UreFD and apo-urease (16).

329 Taken together, our work establishes a paradigm on how cells solve the problem of
330 delivering the nickel ion to urease through complexes of metallochaperones. Nickel ions are
331 delivered within the $UreE_2G_2$ complex and the activation complex so that the toxic metal ions
332 do not escape to the cytoplasm. Our work also reveals how GTP and nickel binding
333 allosterically regulate the formation and dissociation of the complexes so that the
334 metallochaperone can shuttle the metal ions to the next protein target along the urease
335 maturation pathway.

336

337 **Materials and Methods**

338 **Protein Expression and Purification**

339 The *H. pylori* apo-urease, $UreGFD_{str}$ complex, and UreG were expressed and purified as
340 described previously (13, 16). To prepare protein samples of *H. pylori* UreE and its truncation
341 variants, the coding sequences of wild-type (residues 1-170) UreE, UreE(1-158) and UreE(1-
342 148) were subcloned into the pET-Duet-1 vector to create pHpUreE, pHpUreE(1-158),
343 pHpUreE(1-148), respectively (Fig. S10). These plasmids were then transformed to *E. coli*
344 Rosetta (DE3) pLysS. Bacterial cultures were grown in Terrific Broth with 100 μg/ml
345 ampicillin and 25 μg/ml chloramphenicol to an OD_{600} of 0.6 and induced with 1 mM
346 isopropyl β-D-1-thiogalactopyranoside (IPTG) at 25 °C overnight. Four grams of harvested
347 cells were suspended in buffer SP [20 mM HEPES, pH 6.8, 1 mM Tris(2-
348 carboxyethyl)phosphine hydrochloride (TCEP)] supplemented with 0.1 g of complete
349 ULTRA Tablets protease inhibitor cocktail (Roche) and lysed by sonication. Following
350 centrifugation (20,000 g, 45 min), the supernatant was loaded onto a 5 mL HiTrap SP HP
351 cation exchange column pre-equilibrated with the buffer SP. After washing with 120 mM
352 NaCl in the buffer SP, UreE were eluted using 330 mM NaCl in buffer SP. To remove any
353 bound metal ions in the UreE sample, 1 mM ethylenediaminetetraacetic acid (EDTA) was
354 added to the protein samples, which were then loaded to a HiLoad Superdex 75 PG gel
355 filtration chromatography column pre-equilibrated with the assay buffer (20 mM HEPES, pH
356 7.5, 200 mM NaCl, 1 mM TCEP).

357 To prepare protein samples of the $UreE_2G_2$ complex, 150 μM of UreE(1-158) or UreE(1-
358 148) were mixed and 150 μM UreG in the assay buffer supplemented with 2 mM $NiSO_4$, 4
359 mM $MgSO_4$, and 5 mM 5'-guanylyl imidodiphosphate (GMPPNP), and purified by loading to
360 a HiLoad Superdex 200 PG gel filtration chromatography column pre-equilibrated in the
361 assay buffer.

362 To prepare protein samples of $HypA_{str}$, the coding sequences of the Strep-tag II
363 (WSHPQFEK) were added to the C-terminus of *H. pylori* HypA and subcloned into the
364 pRSETA vector to create $pHpHypA_{str}$ (Fig. S10). The plasmid was transformed into *E. coli*
365 Rosetta (DE3) pLysS. Bacterial cultures were grown in Terrific Broth with 100 μg/ml
366 ampicillin and 25 μg/ml chloramphenicol to an OD_{600} of 0.6 and induced with 1 mM IPTG at
367 25 °C overnight. Three grams of harvested cells were suspended in the Strep-binding buffer
368 (50 mM HEPES, pH 7.5, 200 mM NaCl, and 1 mM TCEP) supplemented with 0.1 g of
369 complete ULTRA Tablets protease inhibitor cocktail (Roche) and lysed by sonication. After
370 centrifugation at 20,000 g, 45 min, the supernatant was loaded onto a Strep-Tactin XT 4Flow
371 affinity column (IBA Lifesciences) pre-equilibrated with the Strep-binding buffer. $HypA_{str}$
372 were eluted using 50 mM biotin in strep binding buffer.

373 To prepare protein samples of Ni(II)-bound UreE and Ni(II)-bound $HypA_{str}$, 1 mM
374 $NiSO_4$ was added to 200 μM samples of UreE, UreE(1-158), UreE(1-148) or $HypA_{str}$, which
375 were then loaded to a Superdex 75 10/300 gel filtration chromatography column
376 preequilibrated with the assay buffer to remove the excess $NiSO_4$.

377 **Protein Crystallization and Structure Determination**

378 Two millimolar $NiSO_4$, 4 mM $MgSO_4$, and 5 mM GMPPNP were added to 170 μM
379 protein samples of $UreE(1\text{-}158)_2G_2$ or $UreE(1\text{-}148)_2G_2$ complex. The protein samples and the
380 reservoir solution (0.2 M sodium malonate dibase monohydrate, 0.1 M bis-tris propane, and
381 18% PEG3350, pH 6.1) were mixed in a 2:1 volume ratio on a cover slip for hanging drop
382 vapor diffusion at 16 °C. Crystals were cryoprotected by soaking 10% of glycerol and flash
383 frozen in liquid nitrogen. For the $UreE(1\text{-}148)_2G_2$ complex, diffraction data was collected at
384 1.5418 Å using an in-house X-ray generator (Rigaku FRE+) and a RAXIS IV imaging plate
385 detector. For the $UreE(1\text{-}158)_2G_2$ complex, crystal diffraction data was collected at the
386 absorption peak of nickel at 1.477 Å on the TPS05A beam line of NSRRC. Diffraction data

387 were indexed and integrated using the program XDS (25) and scaled with AIMLESS in the
388 CCP4 suite (26). For the UreE(1-158)$_2$G$_2$ complex, phases were determined by MR-SAD
389 using the crystal structure of Ni-bound UreE (11) (PDB code: 3tj8) as the search template. For
390 the UreE(1-148)$_2$G$_2$ complex, phases were determined by the molecular replacement method
391 using the structure of the UreE(1-158)$_2$G$_2$ complex as the search template. Models were built
392 interactively using the program COOT (27) and refined using the programe
393 PHENIX.REFINE (28). Figures of protein structures were created using PyMOL
394 (www.pymol.org).

395 **Pull-down assay**

396 For the pull-down assay in Fig. 5B, 150 μM of UreE or its truncation variants and 150
397 μM of HypA$_{str}$ were added to 0.1 mL Strep-Tactin XT 4Flow resin pre-equilibrated with the
398 Strep-binding buffer in a spin column. After washing with 0.4 mL Strep-binding buffer,
399 proteins were eluted with 50 mM biotin in the Strep-binding buffer, analyzed by SDS-PAGE,
400 and stained with Coomassie Blue.

401 **In-vitro urease activation assay**

402 We reconstructed the urease maturation pathway in vitro using purified protein samples
403 (Fig. S11). For the urease activation assay in Fig. 4B, 40 μM of Ni-bound UreE, UreE(1-158)
404 or UreE(1-148) were added to 10 μM of apo-urease, 40 μM of UreGFD$_{str}$ in the reaction
405 buffer (20 mM HEPES, pH 7.5, 200 mM NaCl, 1 mM TCEP, 2 mM $MgSO_4$ and 300 μM
406 GTP). For the urease activation assay in Fig. 5C, 40 μM Ni-bound HypA$_{str}$ was added to 10
407 μM of urease, 40 μM of UreGFD$_{str}$, 40 μM of UreE, UreE(1-158) or UreE(1-148) in the
408 reaction buffer. For negative controls, apo-forms of UreE or HypA$_{str}$ were added instead of
409 Ni(II)-bound UreE or Ni(II)-bound HypA$_{str}$. To stimulate GTP hydrolysis of UreG required
410 for urease activation, 10 mM of $KHCO_3$ was added to the reaction mixture and incubated at

411 37°C for 30 min. To measure the urease activity, 50 mM urea was added to the reaction
412 mixture and incubated at 37°C for 30 min and the amount of ammonia released was measured
413 using a phenol/hypochlorite reaction (29).

414 **Urease activation assay in a two-chamber dialyzer**

415 20 μM Ni(II)-bound $HypA_{str}$, 40 μM apo-form of UreE, 40 μM $UreGFD_{str}$, and 10 μM
416 apo-urease in the reaction buffer were added to either side of two-chamber dialyzers
417 (Bioprobes Ltd.) separated by a dialysis membrane (3.5 kDa MWCO; Spectrum Labs) as
418 indicated in Fig. 5A. The dialyzers were incubated at 37°C for 60 min with shaking. To
419 stimulate GTP hydrolysis of UreG required for urease activation, 10 mM of $KHCO_3$ was
420 added to the reaction mixture and incubated at 37°C for 30 min. To measure the urease
421 activity, 50 mM urea was added to the reaction mixture from the urease-containing chamber
422 and incubated at 37°C for 20 min. The amount of ammonia released was quantified using a
423 phenol/hypochlorite reaction (Weatherburn 1967).

424

425 **Acknowledgement**

426 This work was supported (in part) by grants from the Research Grants Council of Hong Kong
427 (14117321, 14117223, C4041-18E, C4002-21-EF, C2003-22W, AoE/M-403/16, AoE/M-
428 05/12, AoE/M-402/25-N) and by direct grants from the Chinese University of Hong Kong.
429 Molecular graphics and analyses were performed using PyMOL (https://pymol.org/). We
430 thank the National Synchrotron Radiation Research Center for providing beamline for X-ray
431 data collection.

432

433 **Data deposition**

434 The atomic coordinates and structure factors of the UreE(1-158)$_2$G$_2$ and UreE(1-148)$_2$G$_2$
435 complexes (PDB ID code: 20ZY and 21AD, respectively) were deposited in the Protein Data
436 Bank, www.wwpdb.org.

437 **Figure Legends**

438 **Figure 1. Crystal structures of $UreE_2G_2$ in complex with nickel and GMPPNP.**

439 (A) In the presence of GTP, UreG dissociates from the UreGFD complex and forms a 2:2
440 complex with UreE. UreG gets its nickel ion from the $UreE_2G_2$ complex and then forms an
441 activation complex with UreFD and apo-urease. Upon GTP hydrolysis, the nickel ion is
442 delivered to the active site of urease via a protein tunnel within the activation complex. (B-C)
443 The structures of (B) $UreE(1\text{-}158)_2G_2$ and (C) $UreE(1\text{-}148)_2G_2$ in complex with Ni(II) and
444 GMPPNP were determined at a resolution of 3.10 Å and 2.85 Å, respectively. In the
445 asymmetry unit of $UreE(1\text{-}158)_2G_2$ and $UreE(1\text{-}148)_2G_2$, four and two copies of the $UreE_2G_2$
446 complexes were found, respectively. UreE and UreG dimers are in different shades of orange
447 and blue, respectively. (D) Overall folds of UreE (left panel) and UreG (right panel). The C-
448 terminal tail, N-terminal (NTD) and C-terminal (CTD) domains of UreE are in green, teal and
449 pink, respectively. The G1-G5 and CPH motifs of UreG are in cyan, blue, brown, magenta,
450 orange and green, respectively. (E) UreE and UreG forms an asymmetric 2:2 complex, where
451 (F) His68 of distal UreG moves towards the nickel binding site of UreE and chelates a Ni(II)
452 ion with His102 from both proximal and distal UreE. (G-H) Sequence alignment of UreE and
453 UreG. Sequences of *H. pylori* (Hp), *Sporosarcina pasteurii* (Sp) and *Klebsiella aerogenes*
454 (Ka) UreE and UreG were aligned using the program PROMAL3D (30). The names of the
455 secondary structure elements of UreE and UreG follow those used in references (31) and (12).
456 Residue number, according to the Hp sequences, and secondary structure elements are
457 indicated above the alignment. The NTD, CTD, C-terminal tail of UreE, G1-G5 and CPH
458 motifs of UreG are indicated below the alignment.

459

460

461 **Figure 2. Asymmetric interactions in the $UreE_2G_2$ complex.**

462 (A) UreG dimer (orange) interacts mainly with proximal E (light blue). (B) Residues within 4
463 Å of the UreE-UreG interface are highlighted in light blue (proximal UreE), cyan (distal
464 UreE), light orange (proximal UreG) or orange (distal UreG). Other residues of distal UreE
465 and UreG are in darker shades of gray. Residues that are directly involved in the UreE-UreG
466 interactions are labeled. Apostrophes indicate residues from distal UreE or UreG.

467

468 **Figure 3. GTP-dependent conformational changes in UreG promote binding of distal**
469 **UreG to the $UreE_2G_2$ complex.**

470 (A) Superimposition of proximal (light orange) and distal (orange) UreG with GDP-bound
471 UreG in the UreGFD complex (gray). GMPPNP binding induces conformational changes in
472 the G2 motif (blue) and helix-2 of both proximal and distal UreG. In the distal UreG,
473 additional conformational changes are found in the CPH metal-binding motif (green). (B)
474 Charge repulsion (thick arrow) between the γ-phosphate of GMPPNP and Asp37 induces
475 conformational changes in the G2 motif. As a result, Tyr39 moves towards and forms a
476 hydrogen bond with Glu119 of proximal UreE. The His68 of the CPH motif of distal UreG
477 moves towards UreE and chelates a nickel ion with His102 from both proximal and distal
478 UreE. Hydrogen bonds are indicated by dotted lines. Apostrophes indicate residues from
479 distal UreE or UreG. (C) Conformational changes in the G2 motif cause helix-2 to tilt towards
480 the nucleotide binding site, bringing Asp37, Glu42 and Asp43 of distal UreG to form salt-
481 bridges (dotted lines) to Arg130 and Lys131 of proximal UreG.

482

483

484 **Figure 4. UreG binding induces conformational changes in NTD and the C-terminal tail**
485 **of proximal UreE.**

486 (A) Conformational changes in UreE upon the formation of the $UreE_2G_2$ complex. NTD,
487 CTD and the C-terminal tail of UreE are in teal, pink and green, respectively. Compared to
488 the crystal structure of nickel-bound UreE dimer (PDB: 3tj8; gray), conformational changes
489 are found in the NTD and the C-terminal tail (149-155) of proximal UreE. (B) The NTD of
490 proximal UreE (light blue) undergoes a domain movement such that Ile2, Ile34, Arg36, Ala46
491 and Arg48 form a pocket to accommodate Leu197 of proximal UreG (light orange). Structure
492 of the UreE dimer is in salmon. (C) In the nickel-bound UreE dimer (PDB: 3tj8; salmon),
493 His152 is interacting with a nickel ion at the dimeric interface. Upon the formation of the
494 $UreE_2G_2$ complex, the C-terminal tail of proximal UreE (green) swings outwards such that
495 His152 forms a hydrogen bond with Asp74 of proximal UreG. Residues 156-158 of UreE
496 (dotted lines) are disordered and not involved in binding UreG. (D) The C-terminal tail of
497 UreE is not essential for nickel transfer between UreE and UreG. Ni-bound UreE or its
498 truncation variants were added to a reaction mixture containing GTP, $KHCO_3$, UreGFD and
499 apo-urease. Urease was activated with the addition of Ni-bound UreE or its truncation
500 variants, but not their apo-forms.

501

502 **Figure 5. Interaction between HypA and the C-terminal tail of UreE facilitates nickel**
503 **transfer required for urease maturation.**

504 (A) Ni-bound $HypA_{str}$ (Ni-$HypA_{str}$), UreE, UreGFD and apo-urease in buffer containing 2
505 mM $MgSO_4$ and 300 μM GTP were added to either side of two-chamber dialyzers as
506 indicated. 10 mM $KHCO_3$ was added to activate the GTP hydrolysis of UreG required for
507 urease activation. Urease was activated in A1 where all the protein components for the urease

508 activation were in the same chambers, but not in A2 and A3, where Ni-$HypA_{str}$ and UreE
509 were separated by a dialysis membrane to prevent protein-protein interactions. Our results
510 suggest that UreE was able to receive nickel from Ni-$HypA_{str}$ via protein-protein interactions.
511 (B) The C-terminal tail of UreE is essential for HypA-UreE interaction. UreE and its
512 truncation variants were mixed with $HypA_{str}$ and loaded to Strep-Tactin resins. After
513 extensive washing, bound proteins were eluted with 50 mM biotin. Our results show that
514 truncation of the C-terminal tail of UreE greatly weaken their interactions with $HypA_{str}$. (C)
515 Ni-$HypA_{str}$ was added to UreE or its truncation variants, UreGFD and apo-urease. Apo-form
516 of $HypA_{str}$ was added as negative controls. Our results suggest that the UreE truncation
517 variants failed to receive nickel ions from HypA for urease activation.

518

519 **Figure 6. Structural insights into how conformational changes in the $UreE_2G_2$ complex**
520 **facilitate nickel delivery.**

521 (A) Nickel transfer weakens UreE-UreG interactions. The structure of Ni/GMPPNP-bound
522 UreG dimer (gray; PDB: 5xkt) is superimposed with the distal UreG (orange) in the $UreE_2G_2$
523 complex. In the $UreE_2G_2$ complex, a nickel ion is bound at the UreE binding site by His68 of
524 proximal UreG and His102 of UreE. Transfer of the nickel ion to UreG (green arrow), where
525 it is coordinated by Cys66 and His68, induces conformational changes (black arrows) that
526 break a number of interactions (dashes) between distal UreG and UreE. Apostrophes indicate
527 residues from distal UreE or UreG. (B) The C-terminal tail (red) of UreE is essential in
528 binding and getting its nickel ion from HypA. GTP-dependent conformational changes
529 promote the binding of the UreG dimer to UreE, which causes the C-terminal tail of UreE to
530 flip outwards and promote the dissociation of HypA. The formation of the $UreE_2G_2$ complex
531 facilitates nickel transfer from UreE to UreG, which induces conformational changes in UreG,

532 weakening the UreE-UreG interactions and promoting dissociation of Ni-bound UreG dimer.

533 **References**

534 1. M. Amieva, R. M. Peek, Jr., Pathobiology of Helicobacter pylori-Induced Gastric
535 Cancer. *Gastroenterology* **150**, 64–78 (2016).
536 2. C. Mooney, D. J. Munster, P. F. Bagshaw, R. A. Allardyce, Helicobacter pylori acid
537 resistance. *Lancet* **335**, 1232 (1990).
538 3. E. Jabri, M. B. Carr, R. P. Hausinger, P. A. Karplus, The crystal structure of urease
539 from Klebsiella aerogenes. *Science* **268**, 998–1004 (1995).
540 4. N. C. Ha *et al.*, Supramolecular assembly and acid resistance of Helicobacter pylori
541 urease. *Nat Struct Biol* **8**, 505–509 (2001).
542 5. K. L. Tsang, K. B. Wong, Moving nickel along the hydrogenase-urease maturation
543 pathway. *Metallomics* **14**, mfac003 (2022).
544 6. L. Macomber, R. P. Hausinger, Mechanisms of nickel toxicity in microorganisms.
545 *Metallomics* **3**, 1153–1162 (2011).
546 7. A. W. Foster, D. Osman, N. J. Robinson, Metal preferences and metallation. *J Biol*
547 *Chem* **289**, 28095–28103 (2014).
548 8. D. A. Capdevila, K. A. Edmonds, D. P. Giedroc, Metallochaperones and
549 metalloregulation in bacteria. *Essays Biochem* **61**, 177–200 (2017).
550 9. G. J. Colpas, T. G. Brayman, L. J. Ming, R. P. Hausinger, Identification of metal-
551 binding residues in the Klebsiella aerogenes urease nickel metallochaperone, UreE.
552 *Biochemistry* **38**, 4078–4088 (1999).
553 10. R. Shi *et al.*, Crystal structures of apo and metal-bound forms of the UreE protein
554 from Helicobacter pylori: role of multiple metal binding sites. *Biochemistry* **49**, 7080–
555 7088 (2010).
556 11. K. Banaszak *et al.*, Crystallographic and X-ray absorption spectroscopic
557 characterization of Helicobacter pylori UreE bound to Ni(2)(+) and Zn(2)(+) reveals a
558 role for the disordered C-terminal arm in metal trafficking. *Biochem J* **441**, 1017–1026
559 (2012).
560 12. Y. H. Fong *et al.*, Structure of UreG/UreF/UreH complex reveals how urease
561 accessory proteins facilitate maturation of Helicobacter pylori urease. *PLoS Biol* **11**,
562 e1001678 (2013).
563 13. M. H. Yuen, Y. H. Fong, Y. S. Nim, P. H. Lau, K. B. Wong, Structural insights into
564 how GTP-dependent conformational changes in a metallochaperone UreG facilitate

565 urease maturation. *Proc Natl Acad Sci U S A* **114**, E10890–E10898 (2017).
566 14. Y. H. Fong *et al.*, Assembly of preactivation complex for urease maturation in
567 Helicobacter pylori: crystal structure of UreF-UreH protein complex. *J Biol Chem* **286**,
568 43241–43249 (2011).
569 15. X. Yang, H. Li, T. P. Lai, H. Sun, UreE-UreG complex facilitates nickel transfer and
570 preactivates GTPase of UreG in Helicobacter pylori. *J Biol Chem* **290**, 12474–12485
571 (2015).
572 16. Y. S. Nim *et al.*, Delivering a toxic metal to the active site of urease. *Sci Adv* **9**,
573 eadf7790 (2023).
574 17. X. Yang *et al.*, Nickel translocation between metallochaperones HypA and UreE in
575 Helicobacter pylori. *Metallomics* **6**, 1731–1736 (2014).
576 18. H. Q. Hu, H. T. Huang, M. J. Maroney, The Helicobacter pylori HypA.UreE(2)
577 Complex Contains a Novel High-Affinity Ni(II)-Binding Site. *Biochemistry* **57**, 2932–
578 2942 (2018).
579 19. J. W. Olson, N. S. Mehta, R. J. Maier, Requirement of nickel metabolism proteins
580 HypA and HypB for full activity of both hydrogenase and urease in Helicobacter
581 pylori. *Mol Microbiol* **39**, 176–182 (2001).
582 20. S. L. Benoit, A. L. Zbell, R. J. Maier, Nickel enzyme maturation in Helicobacter
583 hepaticus: roles of accessory proteins in hydrogenase and urease activities.
584 *Microbiology (Reading)* **153**, 3748–3756 (2007).
585 21. R. C. Johnson, H. Q. Hu, D. S. Merrell, M. J. Maroney, Dynamic HypA zinc site is
586 essential for acid viability and proper urease maturation in Helicobacter pylori.
587 *Metallomics* **7**, 674–682 (2015).
588 22. H. Q. Hu, R. C. Johnson, D. S. Merrell, M. J. Maroney, Nickel Ligation of the N-
589 Terminal Amine of HypA Is Required for Urease Maturation in Helicobacter pylori.
590 *Biochemistry* **56**, 1105–1116 (2017).
591 23. S. L. Benoit, J. L. McMurry, S. A. Hill, R. J. Maier, Helicobacter pylori hydrogenase
592 accessory protein HypA and urease accessory protein UreG compete with each other
593 for UreE recognition. *Biochim Biophys Acta* **1820**, 1519–1525 (2012).
594 24. B. Zambelli *et al.*, The structure of the high-affinity nickel-binding site in the Ni,Zn-
595 HypA*UreE2 complex. *Metallomics* **15** (2023).
596 25. W. Kabsch, Xds. *Acta Crystallogr D Biol Crystallogr* **66**, 125–132 (2010).
597 26. M. D. Winn *et al.*, Overview of the CCP4 suite and current developments. *Acta*
598 *Crystallogr D Biol Crystallogr* **67**, 235–242 (2011).

599 27. P. Emsley, K. Cowtan, Coot: model-building tools for molecular graphics. *Acta*
600 *Crystallogr D Biol Crystallogr* **60**, 2126–2132 (2004).
601 28. P. D. Adams *et al.*, PHENIX: a comprehensive Python-based system for
602 macromolecular structure solution. *Acta Crystallogr D Biol Crystallogr* **66**, 213–221
603 (2010).
604 29. M. W. Weatherburn, Phenol-Hypochlorite Reaction for Determination of Ammonia.
605 *Anal Chem* **39**, 971 (1967).
606 30. J. Pei, M. Tang, N. V. Grishin, PROMALS3D web server for accurate multiple protein
607 sequence and structure alignments. *Nucleic Acids Res* **36**, W30–34 (2008).
608 31. H. Remaut, N. Safarov, S. Ciurli, J. Van Beeumen, Structural basis for Ni(2+)
609 transport and assembly of the urease active site by the metallochaperone UreE from
610 Bacillus pasteurii. *J Biol Chem* **276**, 49365–49370 (2001).

611

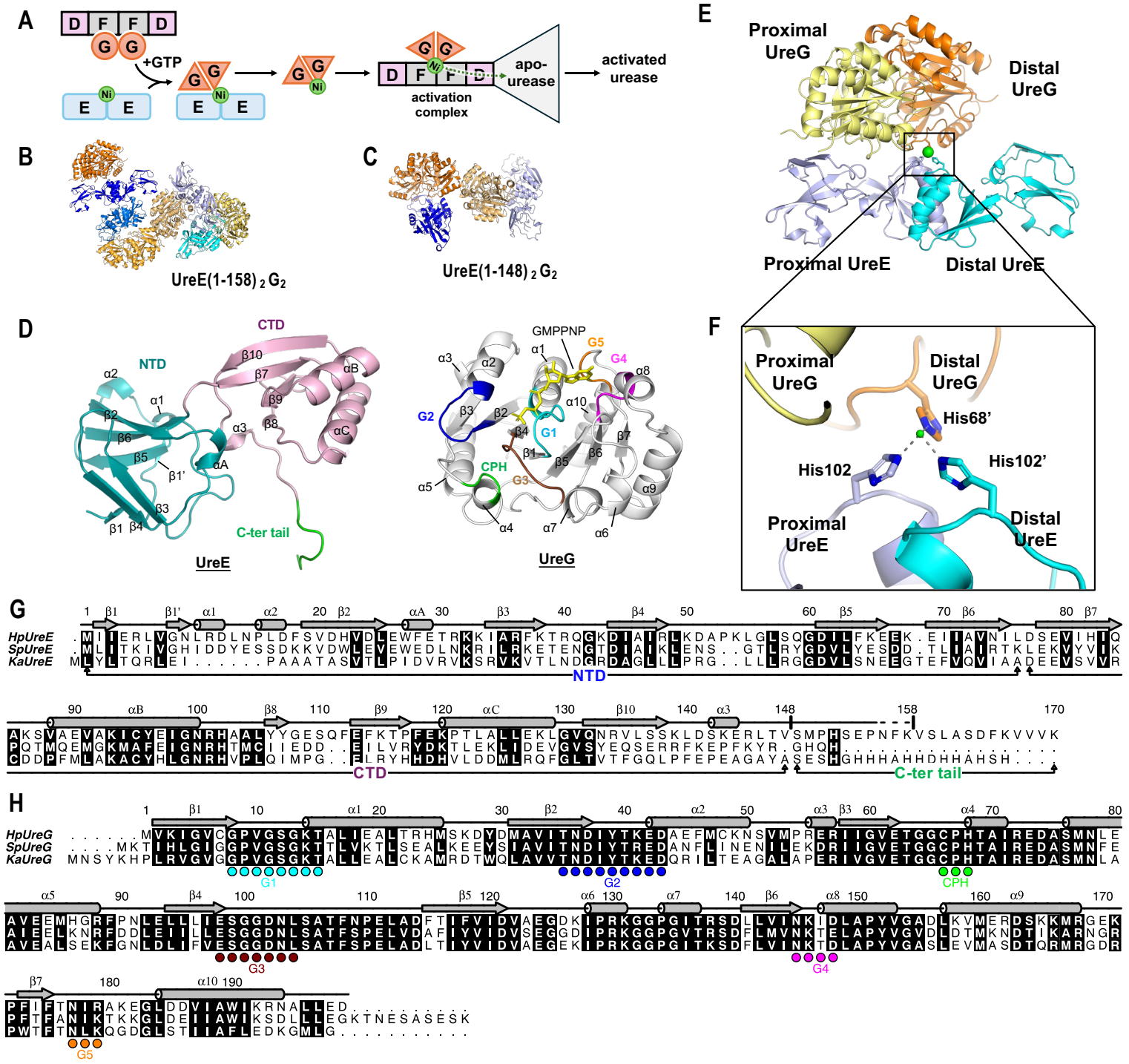

Figure 1. Crystal structures of $UreE_2G_2$ in complex with nickel and GMPPNP.
(A) In the presence of GTP, UreG dissociates from the UreGFD complex and forms a 2:2 complex with UreE. UreG gets its nickel ion from the $UreE_2G_2$ complex and then forms an activation complex with UreFD and apo-urease. Upon GTP hydrolysis, the nickel ion is delivered to the active site of urease via a protein tunnel within the activation complex. (B-C) The structures of (B) $UreE(1\text{-}158)_2G_2$ and (C) $UreE(1\text{-}148)_2G_2$ in complex with Ni(II) and GMPPNP were determined at a resolution of 3.10 Å and 2.85 Å, respectively. In the asymmetry unit of $UreE(1\text{-}158)_2G_2$ and $UreE(1\text{-}148)_2G_2$, four and two copies of the $UreE_2G_2$ complexes were found, respectively. UreE and UreG dimers are in different shades of orange and blue, respectively. (D) Overall folds of UreE (left panel) and UreG (right panel). The C-terminal tail, N-terminal (NTD) and C-terminal (CTD) domains of UreE are in green, teal and pink, respectively. The G1-G5 and CPH motifs of UreG are in cyan, blue, brown, magenta, orange and green, respectively. (E) UreE and UreG forms an asymmetric 2:2 complex, where (F) His68 of distal UreG moves towards the nickel binding site of UreE and chelates a Ni(II) ion with His102 from both proximal and distal UreE. (G-H) Sequence alignment of UreE and UreG. Sequences of *H. pylori* (Hp), *Sporosarcina pasteurii* (Sp) and *Klebsiella aerogenes* (Ka) UreE and UreG were aligned using the program PROMAL3D (30). The names of the secondary structure elements of UreE and UreG follow those used in references (31) and (12). Residue number, according to the Hp sequences, and secondary structure elements are indicated above the alignment. The NTD, CTD, C-terminal tail of UreE, G1-G5 and CPH motifs of UreG are indicated below the alignment.

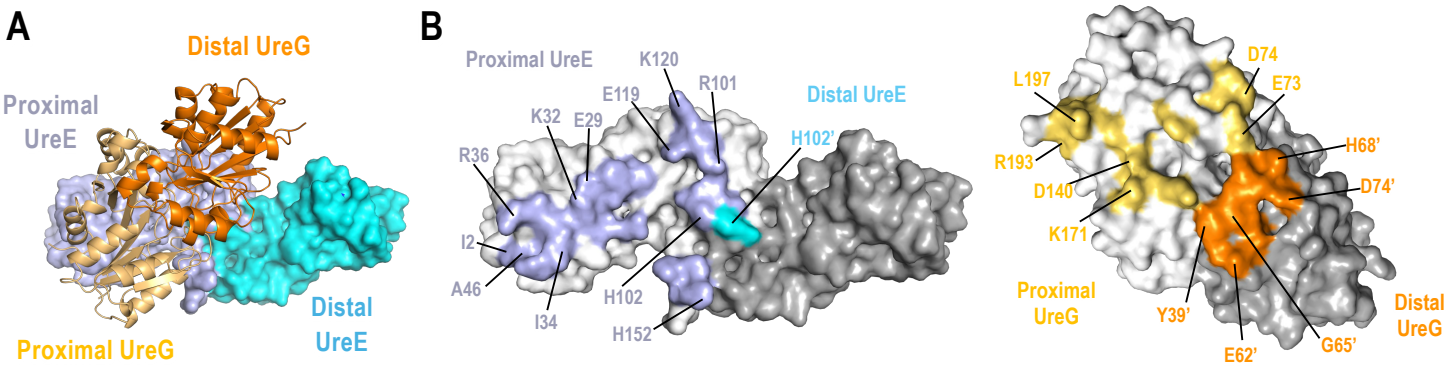

Figure 2. Asymmetric interactions in the $UreE_2G_2$ complex.
(A) UreG dimer (orange) interacts mainly with proximal E (light blue). (B) Residues within 4 Å of the UreE-UreG interface are highlighted in light blue (proximal UreE), cyan (distal UreE), light orange (proximal UreG) or orange (distal UreG). Other residues of distal UreE and UreG are in darker shades of gray. Residues that are directly involved in the UreE-UreG interactions are labeled. Apostrophes indicate residues from distal UreE or UreG.

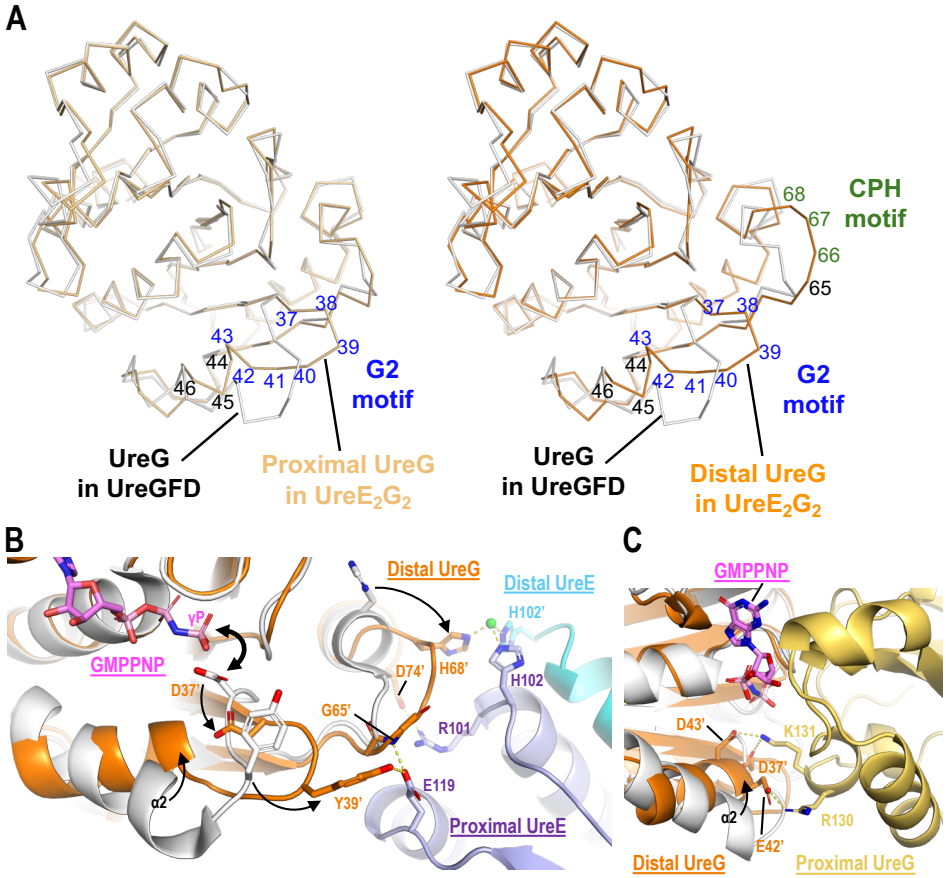

Figure 3. GTP-dependent conformational changes in UreG promote binding of distal UreG to the $UreE_2G_2$ complex.

(A) Superimposition of proximal (light orange) and distal (orange) UreG with GDP-bound UreG in the UreGFD complex (gray). GMPPNP binding induces conformational changes in the G2 motif (blue) and helix-2 of both proximal and distal UreG. In the distal UreG, additional conformational changes are found in the CPH metal-binding motif (green). (B) Charge repulsion (thick arrow) between the γ-phosphate of GMPPNP and Asp37 induces conformational changes in the G2 motif. As a result, Tyr39 moves towards and forms a hydrogen bond with Glu119 of proximal UreE. The His68 of the CPH motif of distal UreG moves towards UreE and chelates a nickel ion with His102 from both proximal and distal UreE. Hydrogen bonds are indicated by dotted lines. Apostrophes indicate residues from distal UreE or UreG. (C) Conformational changes in the G2 motif cause helix-2 to tilt towards the nucleotide binding site, bringing Asp37, Glu42 and Asp43 of distal UreG to form salt-bridges (dotted lines) to Arg130 and Lys131 of proximal UreG.

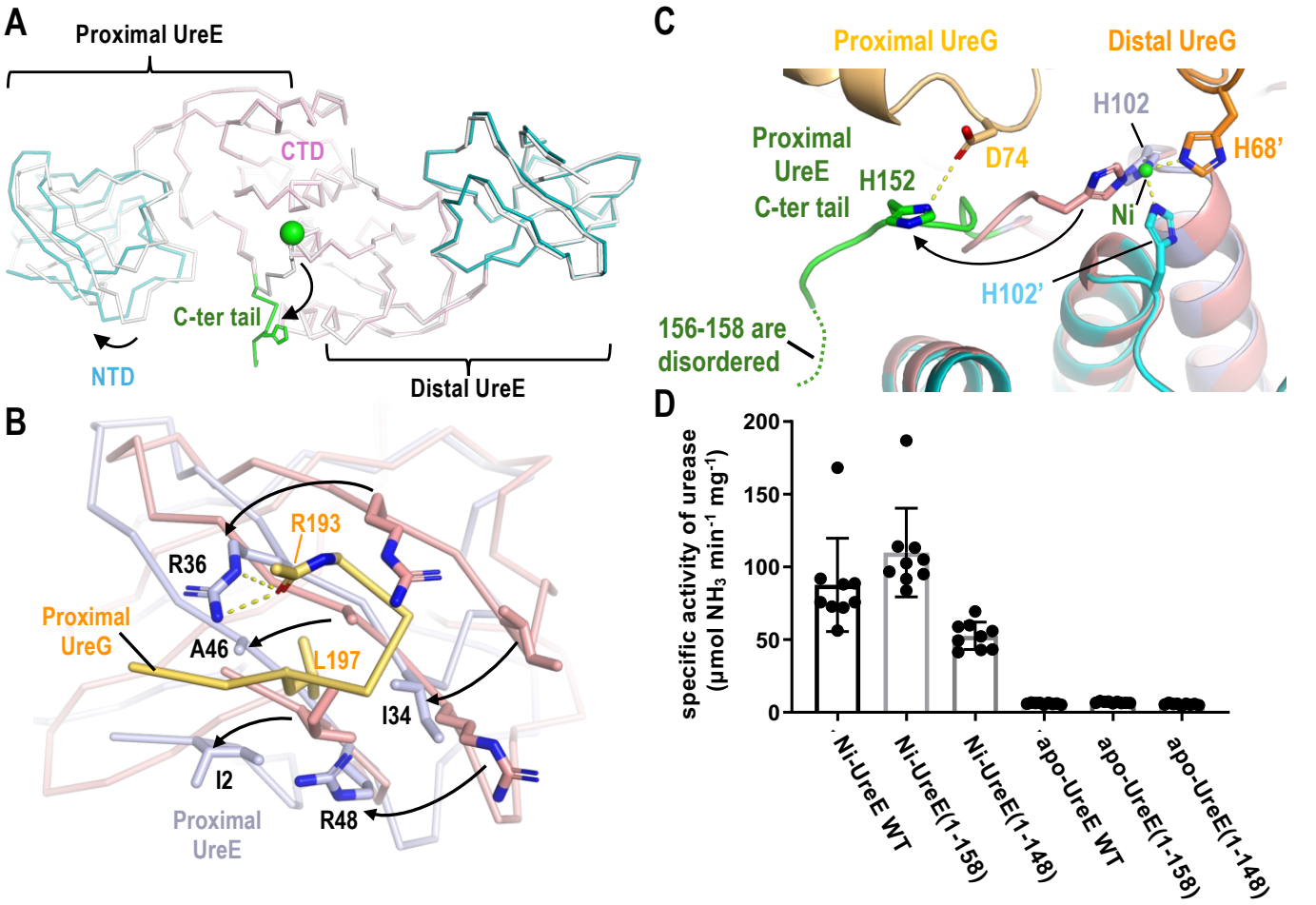

Figure 4. UreG binding induces conformational changes in NTD and the C-terminal tail of proximal UreE.

(A) Conformational changes in UreE upon the formation of the $UreE_2G_2$ complex. NTD, CTD and the C-terminal tail of UreE are in teal, pink and green, respectively. Compared to the crystal structure of nickel-bound UreE dimer (PDB: 3tj8; gray), conformational changes are found in the NTD and the C-terminal tail (149-155) of proximal UreE. (B) The NTD of proximal UreE (light blue) undergoes a domain movement such that Ile2, Ile34, Arg36, Ala46 and Arg48 form a pocket to accommodate Leu197 of proximal UreG (light orange). Structure of the UreE dimer is in salmon. (C) In the nickel-bound UreE dimer (PDB: 3tj8; salmon), His152 is interacting with a nickel ion at the dimeric interface. Upon the formation of the $UreE_2G_2$ complex, the C-terminal tail of proximal UreE (green) swings outwards such that His152 forms a hydrogen bond with Asp74 of proximal UreG. Residues 156-158 of UreE (dotted lines) are disordered and not involved in binding UreG. (D) The C-terminal tail of UreE is not essential for nickel transfer between UreE and UreG. Ni-bound UreE or its truncation variants were added to a reaction mixture containing GTP, $KHCO_3$, UreGFD and apo-urease. Urease was activated with the addition of Ni-bound UreE or its truncation variants, but not their apo-forms.

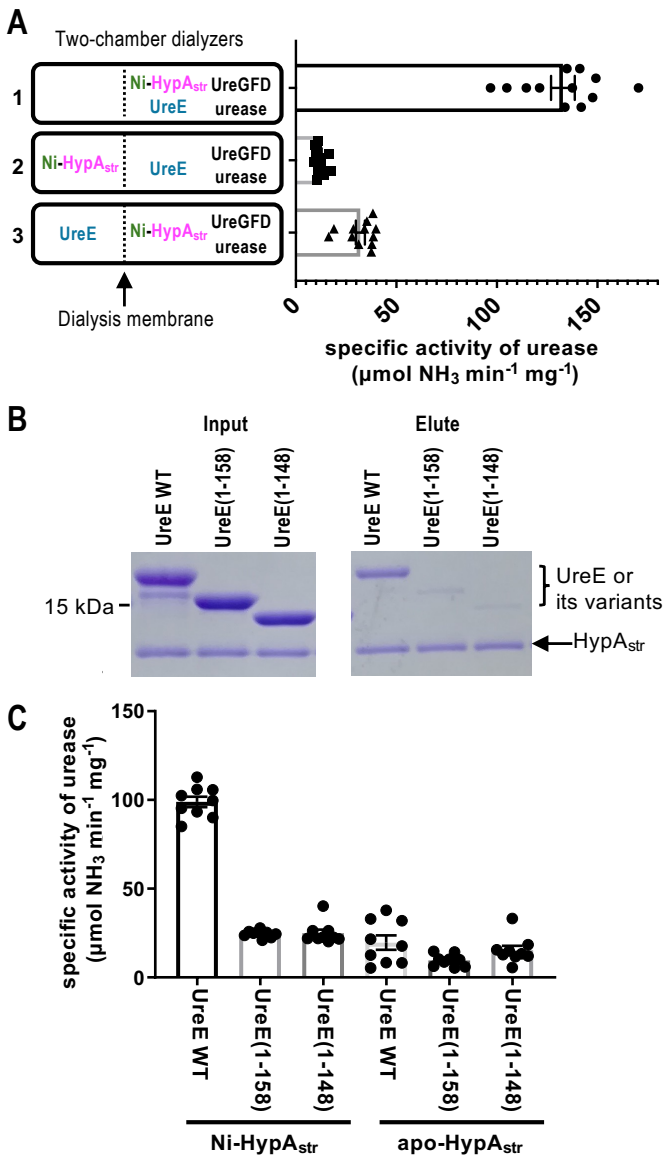

Figure 5. Interaction between HypA and the C-terminal tail of UreE facilitates nickel transfer required for urease maturation.

(A) Ni-bound HypA$_{str}$ (Ni-HypA$_{str}$), UreE, UreGFD and apo-urease in buffer containing 2 mM $MgSO_4$ and 300 μM GTP were added to either side of two-chamber dialyzers as indicated. 10 mM $KHCO_3$ was added to activate the GTP hydrolysis of UreG required for urease activation. Urease was activated in A1 where all the protein components for the urease activation were in the same chambers, but not in A2 and A3, where Ni-HypA$_{str}$ and UreE were separated by a dialysis membrane to prevent protein-protein interactions. Our results suggest that UreE was able to receive nickel from Ni-HypA$_{str}$ via protein-protein interactions. (B) The C-terminal tail of UreE is essential for HypA-UreE interaction. UreE and its truncation variants were mixed with HypA$_{str}$ and loaded to Strep-Tactin resins. After extensive washing, bound proteins were eluted with 50 mM biotin. Our results show that truncation of the C-terminal tail of UreE greatly weaken their interactions with HypA$_{str}$. (C) Ni-HypA$_{str}$ was added to UreE or its truncation variants, UreGFD and apo-urease. Apo-form of HypA$_{str}$ was added as negative controls. Our results suggest that the UreE truncation variants failed to receive nickel ions from HypA for urease activation.

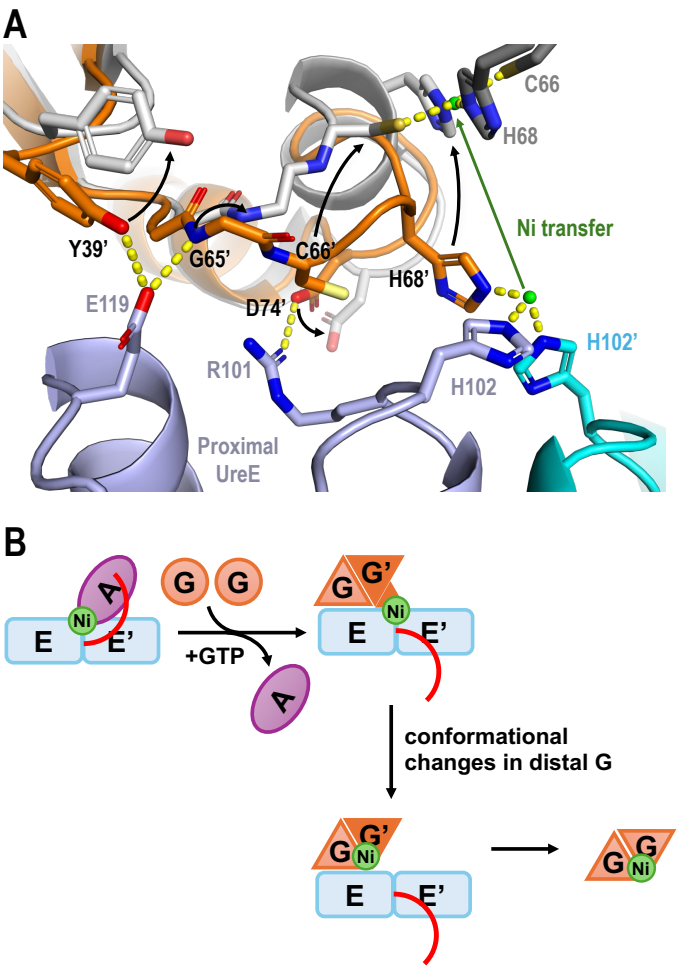

Figure 6. Structural insights into how conformational changes in the $UreE_2G_2$ complex facilitate nickel delivery.

(A) Nickel transfer weakens UreE-UreG interactions. The structure of Ni/GMPPNP-bound UreG dimer (gray; PDB: 5xkt) is superimposed with the distal UreG (orange) in the $UreE_2G_2$ complex. In the $UreE_2G_2$ complex, a nickel ion is bound at the UreE binding site by His68 of proximal UreG and His102 of UreE. Transfer of the nickel ion to UreG (green arrow), where it is coordinated by Cys66 and His68, induces conformational changes (black arrows) that break a number of interactions (dashes) between distal UreG and UreE. Apostrophes indicate residues from distal UreE or UreG. (B) The C-terminal tail (red) of UreE is essential in binding and getting its nickel ion from HypA. GTP-dependent conformational changes promote the binding of the UreG dimer to UreE, which causes the C-terminal tail of UreE to flip outwards and promote the dissociation of HypA. The formation of the $UreE_2G_2$ complex facilitates nickel transfer from UreE to UreG, which induces conformational changes in UreG, weakening the UreE-UreG interactions and promoting dissociation of Ni-bound UreG dimer.

Table S1. Data collection and refinement statistics.

	UreE(1-158)$_2$UreG$_2$	**UreE(1-148)$_2$UreG$_2$**
PDB code	20ZY	21AD
Data collection		
Wavelength (Å)	1.477	1.542
Space group	$P2_1$	$P2_1$
Cell dimensions		
a, b, c (Å)	70.17, 166.60, 154.02	70.97, 151.07, 83.15
α, β, γ (°)	90.00, 90.44, 90.00	90.00, 99.50, 90.00
Resolution (Å)	49.69 – 3.10 (3.18 – 3.10)	46.93 – 2.85 (2.97 – 2.85)
R_{merge}	0.089 (0.592)	0.097 (0.463)
CC(1/2)	0.985 (0.699)	0.995 (0.812)
I/σI	7.1 (1.3)	8.4 (2.4)
Unique reflection no.	62886 (4411)	40155 (4559)
Completeness (%)	98.1 (97.5)	99.6 (100)
Redundancy	2.5 (2.6)	3.6 (3.6)
Refinement		
R_{work} / R_{free}	0.2089 / 0.2448	0.2426 / 0.2719
No. of atoms		
Protein	21509	10356
Ligand/ion	268	134
Water	19	25
B-factors (Å^2)		
Protein	80.31	63.92
Ligand/ion	90.25	48.94
Water	49.76	53.06
r.m.s. deviations		
bond lengths (Å)	0.002	0.003
bond angles (°)	0.483	0.569
Ramachandran		
Favored (%)	98.13	98.66
Allowed (%)	1.87	1.34
Outliers (%)	0.00	0.00

*Values in parentheses are for the highest-resolution shell.

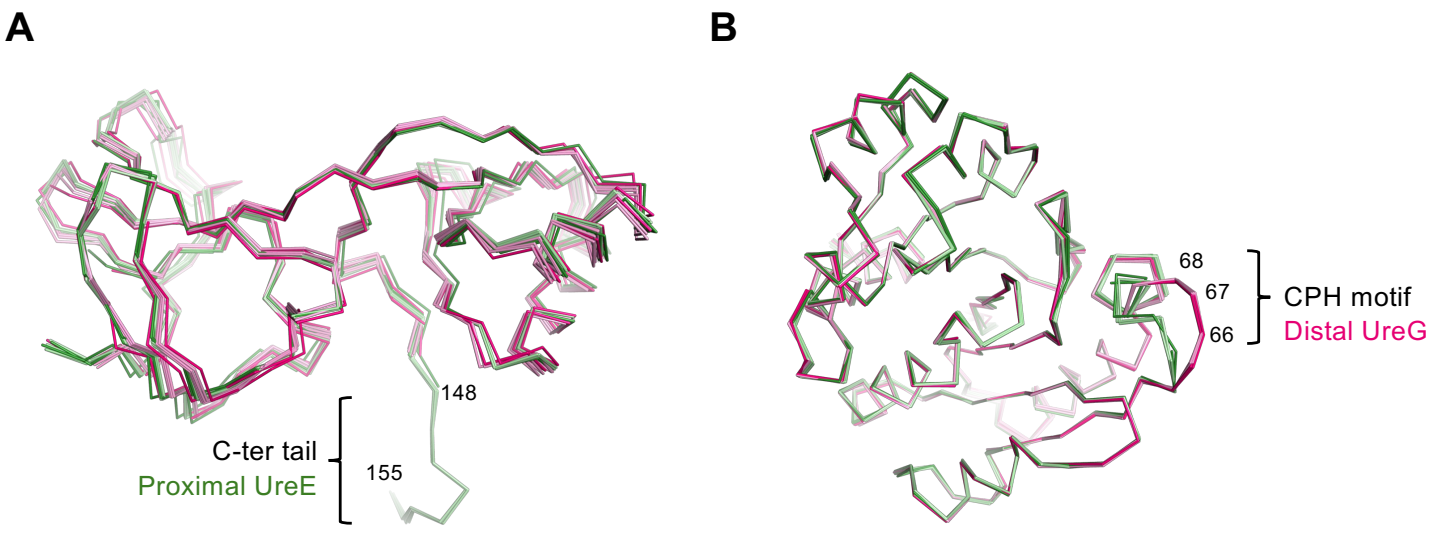

Figure S1. **Structural differences between proximal and distal protomers in the $UreE_2G_2$ complex.** (A) Structures of proximal UreE (green; chain C, G, K, or O) are superimposable to distal UreE (pink; chain D, H, L, or P). Residues (148-155) in the C-terminal tail are structured in the proximal UreE but are disordered in the distal UreE. The structures of $UreE(1\text{-}148)_2UreG_2$ are in darker shades of green and pink. (B) Structures of proximal UreG (green; chain A, E, I, or M) are superimposable to distal UreG (pink; chain B, F, J, or N). The only notable structural differences are found in the metal-binding CPH motif (Cys66-Pro67-His68).

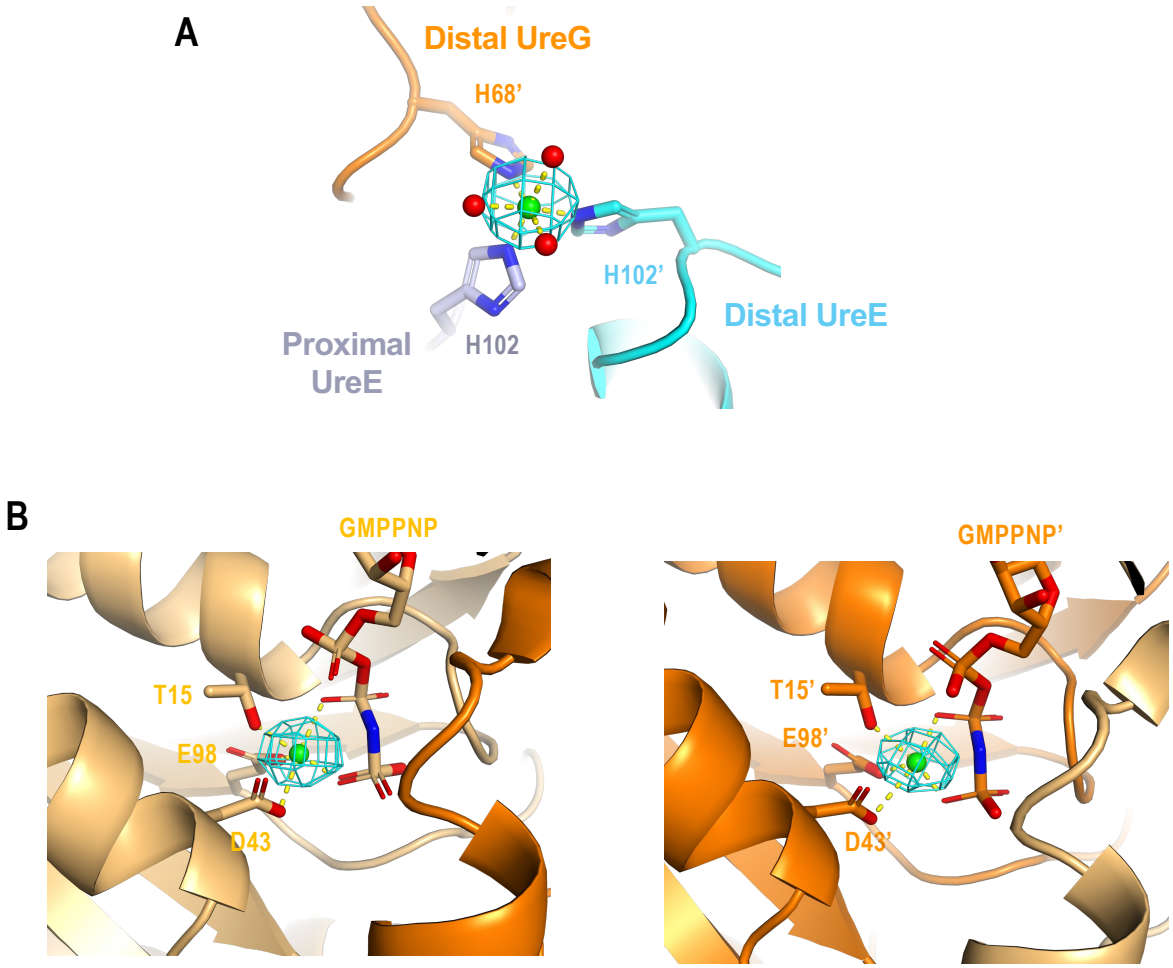

Figure S2. Ni(II) ions identified by anomalous diffraction in the UreE(1-158)$_2$-UreG$_2$ complex. Anomalous difference map (mesh) was generated by PHENIX using diffraction data collected at the nickel peak wavelength and contoured at 7σ. (A) A Ni(II) ion (green) was chelated by His68 of distal UreG, His102 of proximal and distal UreE and three water molecules (red) in an octahedral geometry. (B) Ni(II) ions occupy the Mg(II) binding sites from each of the nucleotide binding sites of proximal (lef) and distal (right) UreG. Apostrophes indicate residues from distal UreE and UreG.

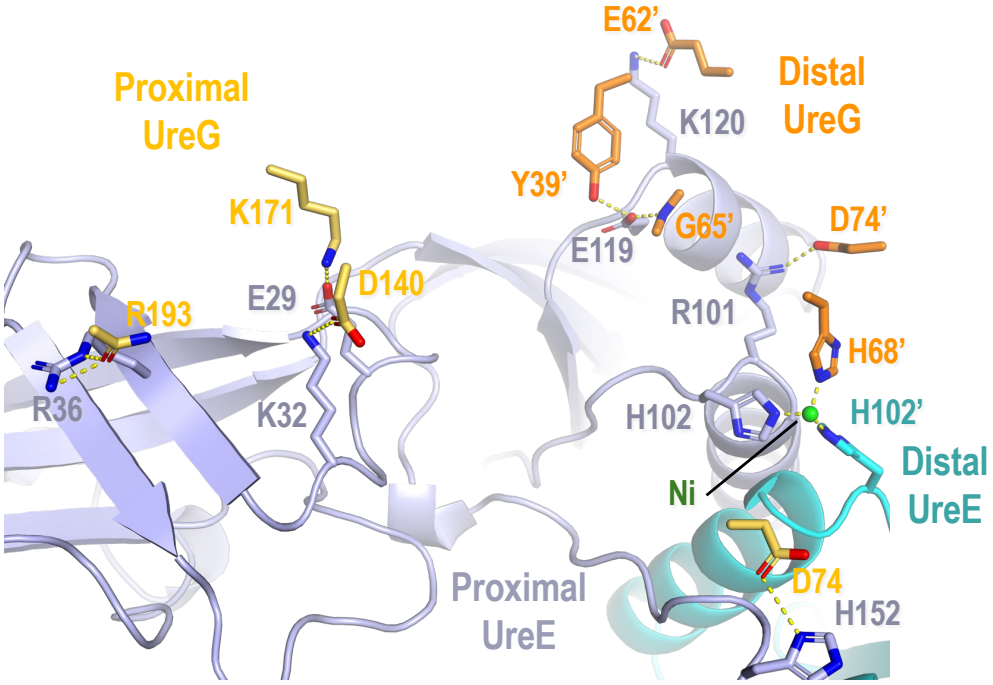

Figure S3. Polar Interactions between UreE and UreG in the $UreE_2G_2$ complex. Residues involved in hydrogen bonds and salt-bridges between UreE and UreG are represented in sticks. Backbone of proximal (light blue) and distal (cyan) UreE are shown as cartoon representation. Residues of proximal and distal UreG are in light orange and orange, respectively. Note that both protomers of UreG mainly interact with proximal UreE. His102', chelating a Ni(II) ion at the interface with His102 of proximal UreE and His68' of distal UreG, is the only residue from distal UreE involved in UreE-UreG interaction. Apostrophes indicate residues from distal UreE or UreG.

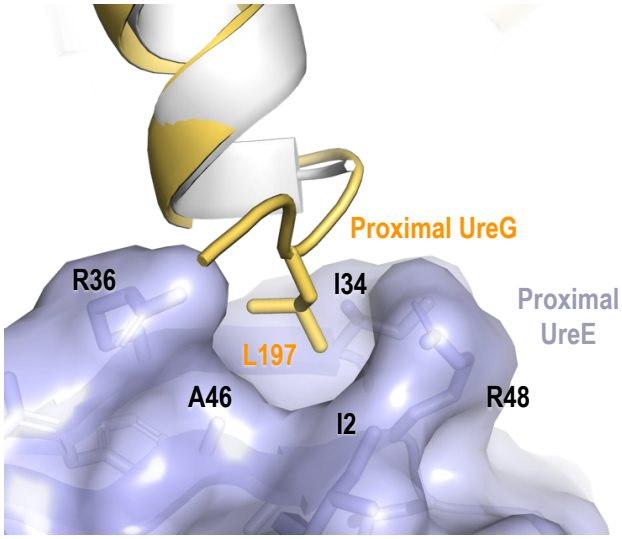

Figure S4. Leu197 of proximal UreG forms hydrophobic interactions proximal UreE. Residue 197-199 of UreG is disordered in the crystal structure of the UreGFD complex (gray) (PDB: 4hi0). These residues become structured in the proximal UreG (light orange) and Leu197 is docked to a hydrophobic pocket formed by Ile2, Ile34, Arg36, Ala46 and Arg48.

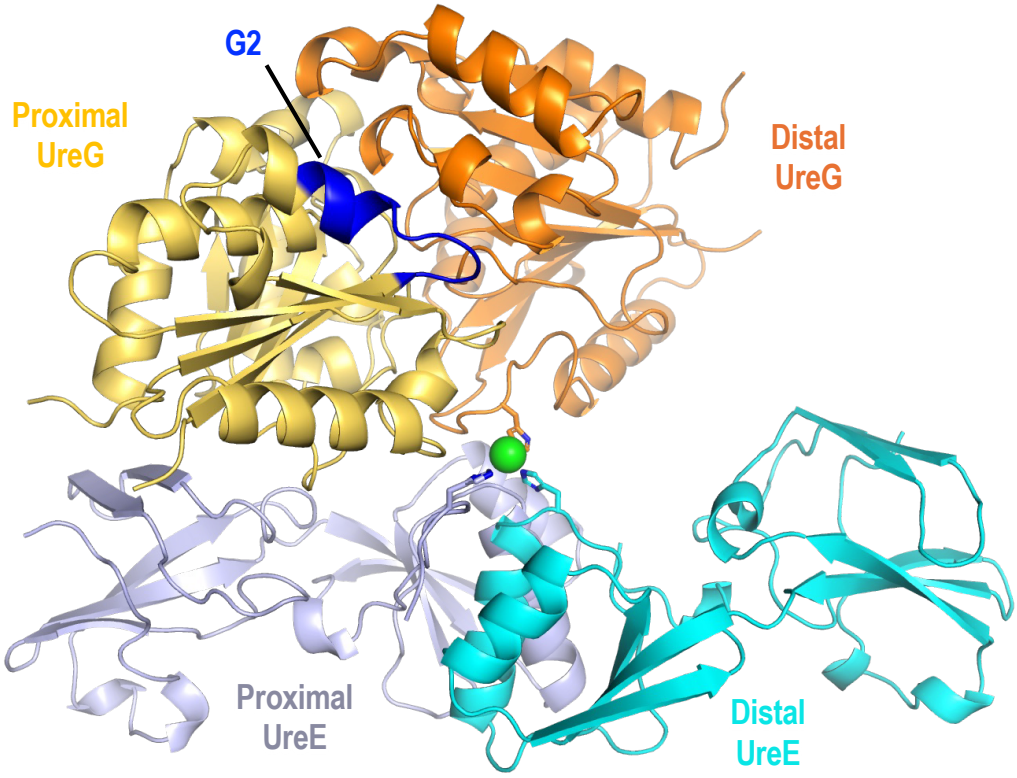

Figure S5. The G2 motif of proximal UreG does not involve in binding UreE. The G2 motif (37-46) of proximal UreG (blue) is located far away from the UreE-UreG interface and does not involve in interacting with UreE.

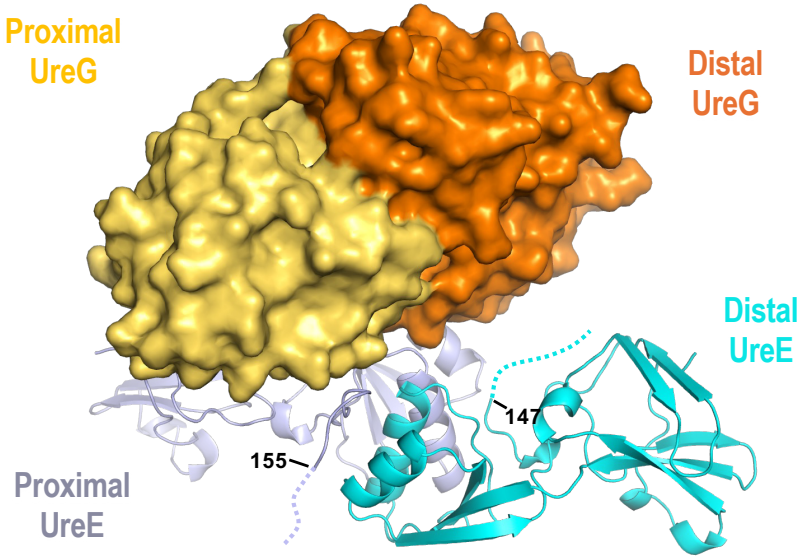

Figure S6. The C-terminal tail of UreE does not involve in binding UreG. In the crystal structure of UreE(1-158)$_2$UreG$_2$, residues 1-155 of proximal UreE and 1-147 of distal UreE are structured. The rest of the C-terminal tails of UreE are disordered and do not involve in binding UreG.

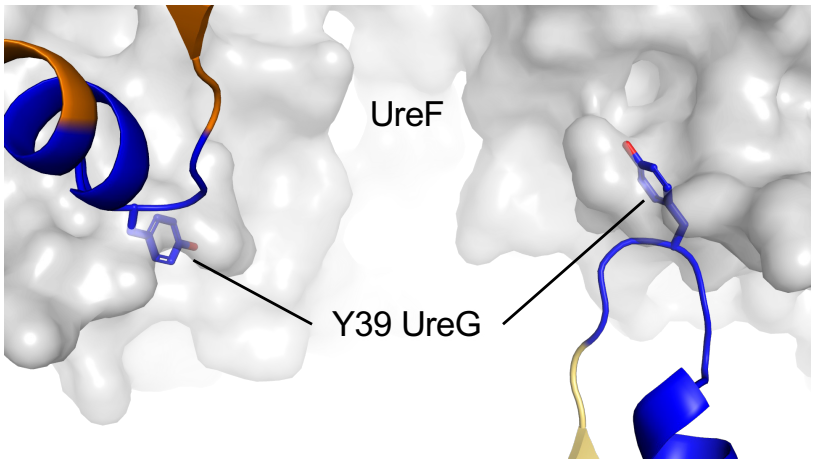

Figure S7. GTP-dependent conformational changes in the G2 motif promotes dissociation of UreGFD complex. GTP binding induces conformational changes in the G2 motif (blue) of UreG such that Tyr39 flips outward and clashes with UreF (gray) in the UreGFD complex. UreF and UreG are in surface and cartoon representations, respectively.

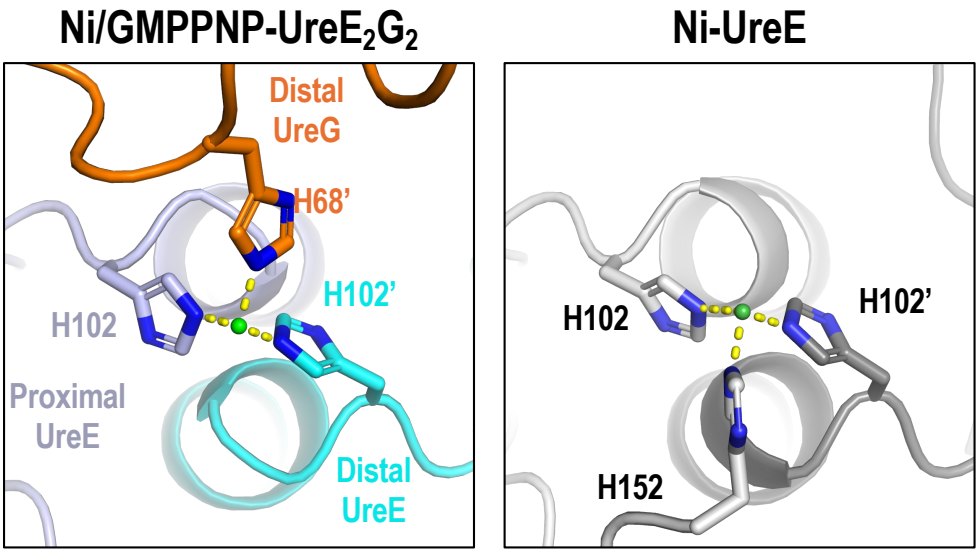

Figure S8. The nickel binding site of the $UreE_2G_2$ complex is the same as that of the UreE. The locations of bound nickel ions in the $UreE_2G_2$ complex (left) and the Ni-bound UreE dimer (right) (PDB: 3tj8) are shown.

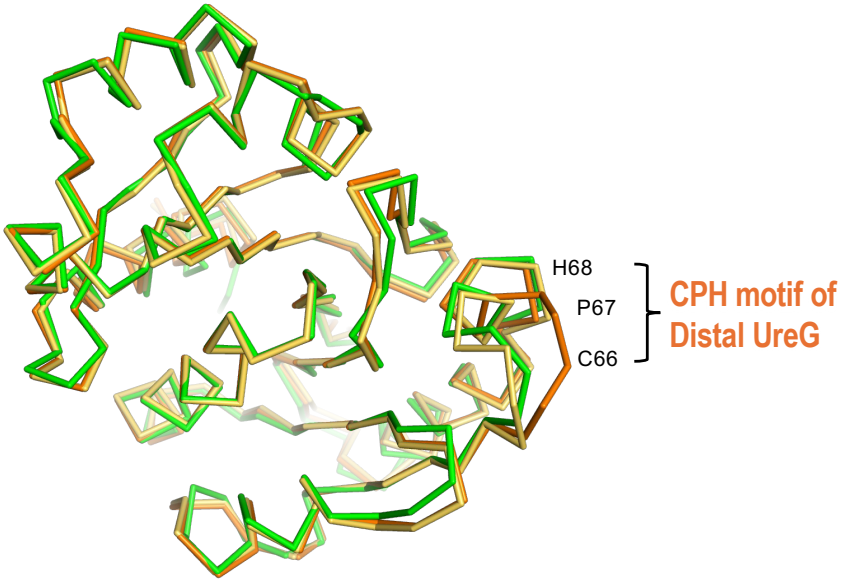

Figure S9. Formation of nickel-bound UreG dimer induce conformational changes in the distal UreG. The structures of proximal (light orange) and distal (orange) UreG were superimposed with Ni/GMPPNP-bound *Klebsiella* UreG (green; PDB: 5xkt). Major conformational changes are found in the CPH motif of the distal UreG.

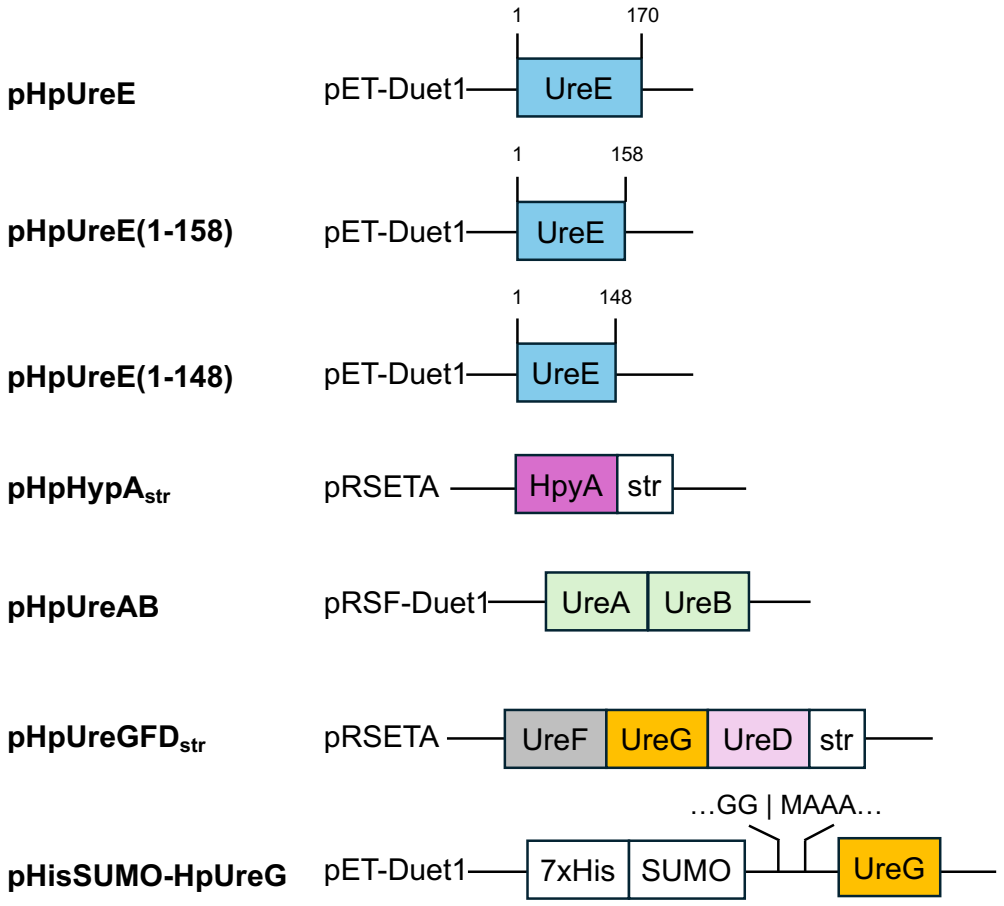

Fig. S10. Summary of expression plasmids used in this study. The names of the plasmids are labeled on the left. str: Strep-tag II sequence (WSHPQFEK); SUMO: Small ubiquitin-like modifier protein; 7xHis: poly-histidine tag. The sequences franking the cutting sites of SUMO protease is labeled.

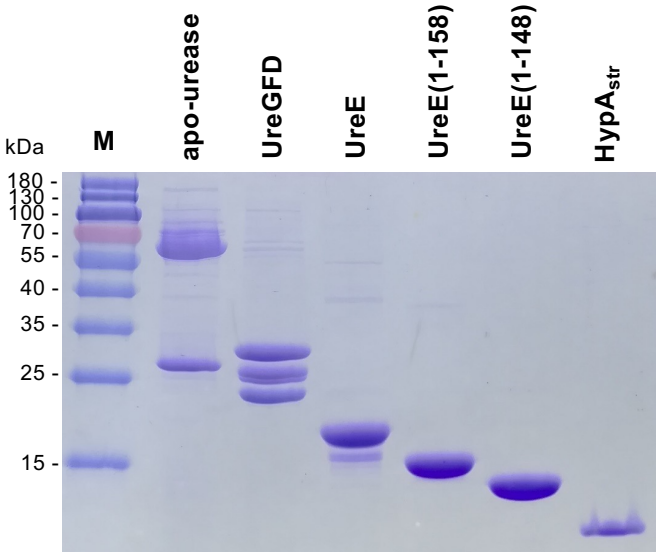

Figure S11. Purified protein samples used in the urease activation and pull-down assays. Purified protein samples of apo-urease, UreGFD, UreE and its truncation variants, HypA$_{str}$ were analyzed by SDS-PAGE stained by Coomassie blue. ThermoFisher PageRuler ™ Prestained Protein Ladder (M) was loaded on the left and the molecular weight of the protein standards were shown.